Photonic Space Switch with Semiconductor Optical Amplifier Using FIR-based Filter and PID Controller

Pedro A. B. Leao, Jonathan A. Soares, M. Rodigheri, T. Sutili, Arismar Cerqueira S. Jr., Evandro Conforti

***Abstract*— This paper presents the proposal and validation of an algorithm to solve equivalent circuits of semiconductor optical amplifiers (SOAs). The developed simulator shows strong agreement with Ansys Circuit results. Building upon this simulator, we investigate the use of two FIR-based filters and a PID controller to reduce switching time and equalize the SOA output signal. Comparisons in terms of rise time and overshoot are presented for all three methods.**

***Keywords*— Equalization, Filters, Optical Space Switches, Semiconductor Optical Amplifier.**

I. Introduction

Semiconductor optical amplifiers (SOAs) are electro-optical devices capable of providing optical gain. This gain arises from carrier population inversion in an electroluminescent structure, enabling stimulated emission of photons by external optical injection. Among the many SOA applications, we highlight wavelength conversion, optical pulse-burst generation, optical carrier suppression/reuse, and the spatial switching of optical signals [1].

In optical-switching scenarios, an SOA can both switch the signals and provide optical gain to the transmitted signal. The primary parameters of interest in such applications include rise time, overshoot, undershoot, and oscillation time. In [2], the pre-impulse step-injected current (PISIC) technique was introduced to reduce SOA switching times, while [3] extends the concept by using multiple impulses (MISIC), combined with an improved microwave design. Additionally, to capture the electrical and optical dynamics, several studies have implemented numerical models matched to experimental data. For instance, [4] presents computational models, supported by experimental measurements, for three different SOAs.

Recently, artificial-intelligence-based algorithms have been explored to reduce rise time, settling time, and overshoot in SOA switching. In [5], a comparative study of particle swarm, ant colony, and genetic algorithms achieved settling times of 542 ps with an overshoot of only 4.8%. Reference [6] further reported settling times below 610 ps and overshoot under 2.2% using the particle swarm optimization (PSO) algorithm.

Building on the small-signal equivalent circuits presented in [4], the present work proposes three approaches to shorten the optical pulse rise time and reduce overshoot in SOA-based switches. The first two methods are based on offline FIR (Finite Impulse Response) pre-filtering of the SOA's electrical drive signal. Finally, a closed-loop PID (Proportional–Integral–Derivative) controller is employed to shape the SOA drive signal [7], [8]. Comparisons are carried out among these three methods. As an additional contribution, we develop and validate a Python-based simulator of equivalent circuits for SOAs.

The article is organized into four sections. Section II discusses in detail the simulations of the SOA equivalent circuit, while Section III presents the results of the proposed algorithms for optical-pulse optimization. Finally, Section IV provides the main conclusions.

Pedro A. B. Leao, Jonathan A. Soares, M. Rodigheri, Evandro Conforti Department of Communications, School of Electrical and Computer Engineering, University of Campinas (UNICAMP), Campinas, SP, Brazil, e-mail: pedrobessaleao@gmail. T. Sutili, Photonics and Quantum Solutions – CPQD Campinas, São Paulo, Brazil. Arismar Cerqueira S. Jr. WOCA Laboratory, National Institute of Telecommunications, e-mail: arismar@inatel.br.

II. Equivalent Circuit Model of the SOA

In this section, we present the construction of the SOA equivalent circuit based on the experimental results shown in [4], followed by a validation procedure using Ansys Circuit software and a custom Python algorithm.

A. Equivalent Model Construction

An SOA can be viewed as a semiconductor laser with highly reduced facet reflectivity. Because of this similarity, our study builds upon the microwave circuit model for semiconductor lasers introduced in [9].

In this model, the chip's resistive (R), inductive (L), and capacitive (C) elements (C_S, R_S, C_{SC}, C_d, R_1, L_S, R_{S1}, and R_{S2}) create electro-optical resonances. The overall impedance of the SOA is also influenced by parasitics in the packaging (C_P, L_P, and R_P). To further improve the model's fidelity, we include additional coupling-circuit elements (R, C_a, L_2, C_2, L_3) and a transmission line, yielding the full equivalent circuit depicted in Fig. 1.

From an experimental setup, the magnitude of the overall system impedance was measured. Using these measurements, we extracted the lumped RLC parameters for three different SOAs (CIP, ETEK, and InPhenix), shown in Table I.

These parameterized SOA models can be applied to simulate a variety of scenarios. In this work, we focus on the SOA's behavior as an optical space switch.

A Python-based algorithm was developed to analyze the equivalent SOA circuits. It implements the circuit in Fig. 1 for each of the three SOA types. Broadly, the algorithm:

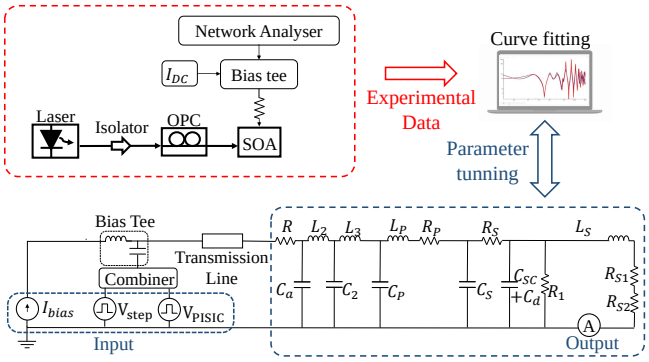

Fig. 1: Schematic representation of the lumped RLC parameter fitting.

TABLE I: Parameters of SOAs CIP, Etek, and InPhenix.

Parameter	SOA CIP	SOA Etek	SOA InPhenix
R (Ω)	46	47	46
C_a (pF)	0.16	0.14	0.20
L_2 (nH)	5.8	7.8	2.7
C_2 (pF)	10	1.8	2.0
L_3 (nH)	1.3	0.7	2.9
C_p (pF)	30	14	1.9
L_p (nH)	1.23	0.4	1.0
R_p (Ω)	0.6	0.2	0.5
C_s (pF)	1	1	1
R_s (Ω)	0.5	0.5	0.5
C_{sc} (pF)	200	200	200
C_d (pF)	400	400	400
R_1 (Ω)	9	9	9
L_s (nH)	0.11	0.11	0.11
R_{s1} (Ω)	0.45	0.45	0.45
R_{s2} ($\mu\Omega$)	6	6	6

- Computes the Fast Fourier Transform (FFT) of input signals,
- Builds the nodal admittance (Y) matrix and source vector (voltage/current) at each frequency,
- Stamps all relevant elements (e.g., RF components, bias tee, coaxial line, SOA parameters) into the Y matrix,
- Solves the frequency-domain system to obtain the output current,
- Performs the Inverse Fast Fourier Transform (IFFT) to reconstruct the time-domain output current.

To validate this custom tool, we compared our results with those from the commercial software Ansys Circuit. The main inputs are time-domain signals (a step voltage plus a bias current), together with the coaxial line, bias-tee, and SOA characteristics, plus the sampling rate.

B. Validation of the Equivalent Model

Three case studies were conducted to validate the Python implementation:

1) Equivalent circuit without transmission line, using a step input,
2) Equivalent circuit with a 5 cm transmission line, using a step input,
3) Equivalent circuit with the same 5 cm line, using both a step input and a PISIC signal.

First, the circuit was simulated without a transmission line. The input was a 5 V step from 2 ns to 7 ns, while a constant 85 mA bias current was maintained (Fig. 2). Under these conditions, the rise times for the InPhenix, CIP, and ETEK SOAs were found to be 0.42 ns, 0.37 ns, and 0.48 ns, respectively, with corresponding overshoot values of 7.62%, 28.10%, and 6.35%.

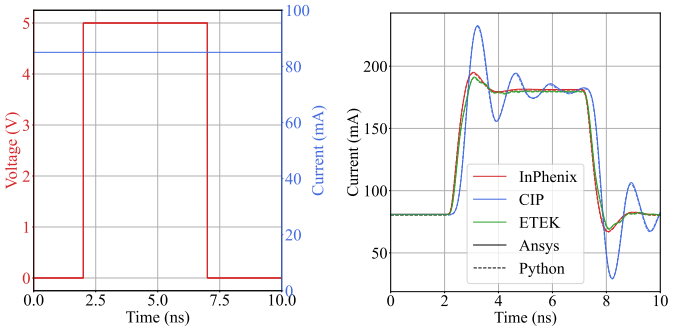

(a) (b)

Fig. 2: Simulation 1 (no transmission line) with a step input: (a) input voltage and bias current; (b) output current.

Next, we introduced a 5 cm transmission line while maintaining the same bias current and step voltage. In Fig. 3, a noticeable delay appears, corresponding to the propagation along the line. In this scenario, the rise times for the InPhenix, CIP, and ETEK devices became 0.35 ns, 0.32 ns, and 0.41 ns, respectively, while the overshoot values were 4.20%, 27.97%, and 2.84%, respectively.

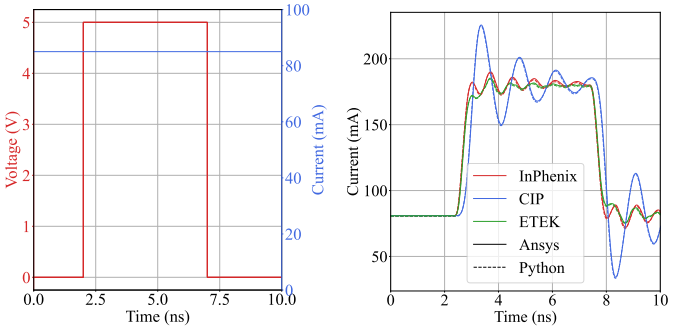

(a) (b)

Fig. 3: Simulation 2 (5 cm transmission line) with a step input: (a) input voltage and bias current; (b) output current.

Finally, to validate the PISIC-technique combiner, we injected a step input supplemented by a short current pulse (PISIC) starting at 2 ns and lasting 1 ns. A 3 dB loss was assumed in the combiner. In this case, based on the results shown in Fig. 4, the rise times dropped to 0.27 ns (InPhenix), 0.27 ns (CIP), and 0.28 ns (ETEK). As expected, the overshoot also increased, reaching 9.78%, 39.11%, and 8.70% for the three SOAs, respectively. Overall, good agreement was observed between the custom Python solver and Ansys Circuit.

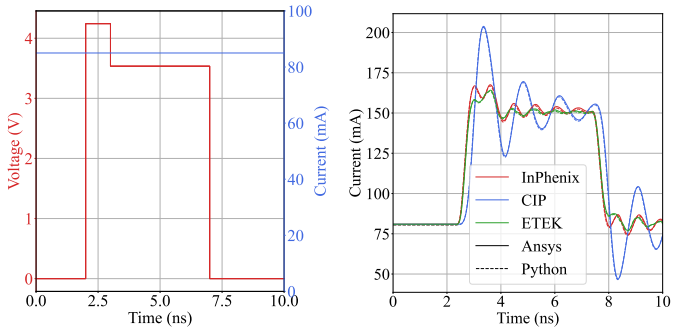

(a) (b)

Fig. 4: Simulation 3 (5 cm transmission line) with a step input plus a PISIC pulse: (a) input voltage and bias current; (b) output current.

III. Techniques for Improving the Optical Pulse

Three different approaches were explored in order to reduce the rise time and overshoot of the optical pulse produced by SOAs. The first two methods rely on offline FIR pre-filtering of the SOA's electrical drive signal, while the third method investigates the use of a PID closed-loop controller.

A. FIR-Based Pre-Filtering of the Signal

In the first approach, we employ a FIR filter to pre-filter the SOA drive signal in an attempt to invert the SOA channel response, denoted by $h[n]$. The idea is to compensate, in advance, for the distortions introduced by the physical SOA equivalent circuit, so that the output optical pulse is equalized. Figure 5 schematically illustrates this procedure.

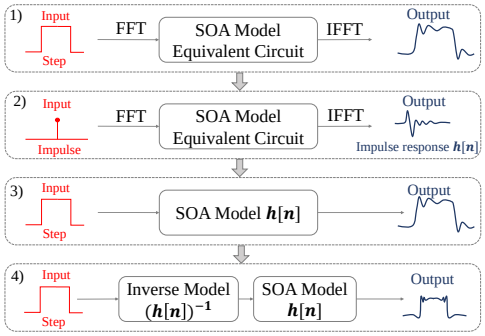

Fig. 5: Block diagram for obtaining and applying the inverse impulse response.

By definition, the impulse response $h[n]$ of a system is the output observed when the input is a unit impulse. Accordingly, we feed a discrete-time impulse (one nonzero sample) into the equivalent circuit and record its output as $h[n]$. To validate this impulse-based approach, we compare two scenarios using a step input:

- The full equivalent circuit solved in the frequency domain,
- The time-domain convolution of the same step input with $h[n]$.

Figure 6 shows excellent agreement between the two methods.

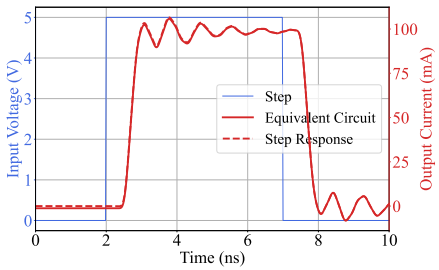

Fig. 6: Comparison between the frequency-domain circuit solution and the time-domain convolution of the step input with $h[n]$.

1) Inverse FIR Filter for the SOA Model: After obtaining $h[n]$, we compute its inverse impulse response $h_{\text{inv}}[n]$ to equalize the SOA output. Figure 7 illustrates both $h[n]$ and one example of its inverse filter. A minimum-phase system is both causal and stable, with all transfer-function zeros lying strictly inside the unit circle [10]. In our case, the circuit response is not strictly minimum-phase, so we use approximate strategies for inversion.

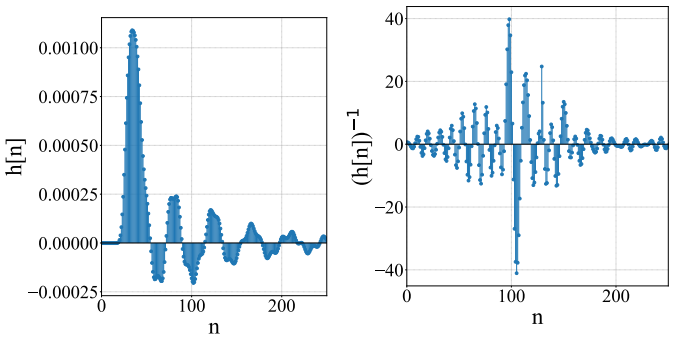

(a) (b)

Fig. 7: Filter 1: (a) measured impulse response of the SOA circuit; (b) a complex (non-minimum-phase) inverse.

One common formulation for the inverse filter exploits the regularized least-squares approach, as illustrated in (1):

$$H_{\text{inv}}(f) = \frac{H^*(f)}{|H(f)|^2 + \varepsilon}, \tag{1}$$

where $H(f)$ is the Fourier transform of $h[n]$, ε is a small regularization factor, and $H_{\text{inv}}(f)$ is the frequency-domain representation of the inverse [10]. This method helps avoid division by near-zero values of $|H(f)|$, but typically introduces additional delay in the overall system response.

Because the circuit is not strictly minimum-phase, the inverse filter tends to be noncausal or exhibits extra oscillatory components at the beginning and end of the filtered waveform. Although this filter successfully reduces rise time, overshoot, and settling time, it imposes latency proportional to the filter length. Figure 8 shows an example of the resulting magnitude response after combining $h[n]$ with its inverse, and Fig. 9 displays the time-domain waveforms.

In Fig. 9, the inverse-filtered step drive shows noticeable pulses near the edges, mimicking the PISIC/MISIC approach

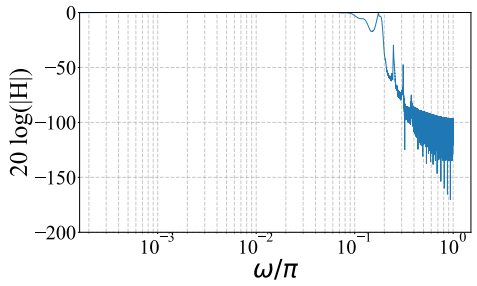

Fig. 8: Overall magnitude response $H_{\text{inv}}(f) \cdot H(f)$. Perfect inversion would be flat, but non-minimum-phase effects remain.

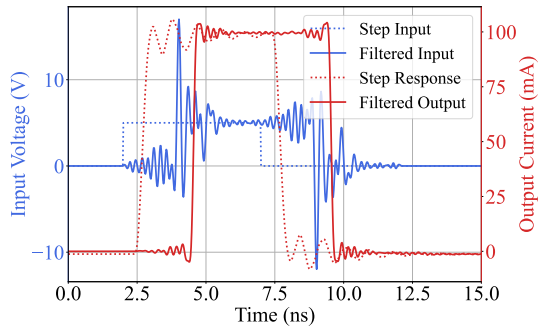

Fig. 9: Resulting input (*filtered* step) and output waveforms after applying the offline inverse filter. Note the reduced rise time but added delay.

by injecting additional energy exactly where the SOA requires it. The output current step is consequently more "square," with lower overshoot and faster settling. However, an obvious latency appears before the output rises, tied to the FIR filter's length.

2) Forcing Causality and Minimum Phase: To reduce the extra delay, one can shift or "roll" the inverse impulse response so that it commences near its most significant amplitude peak. This approach approximates a causal filter by discarding or moving the earlier noncausal portion of the impulse response. Figure 10 shows an example of an inverse FIR constrained to have a near-minimum phase characteristic by suitable windowing and phase adjustment.

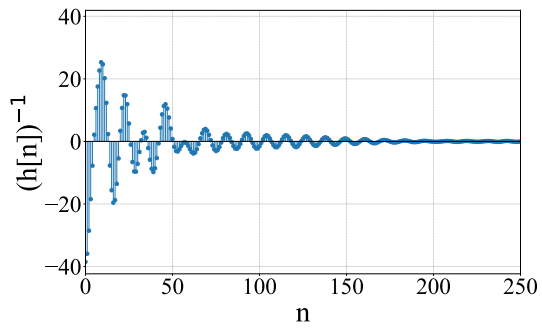

Fig. 10: Example of an inverse FIR filter designed by matching only the magnitude response and forcing near-minimum-phase behavior.

This causal, magnitude-based inverse filter often yields a lower rise time but tends to increase overshoot, since it pushes any "pre-cursor" energy to the very beginning of the pulse. As shown in Fig. 11, these techniques resemble the PISIC/MISIC strategies: they achieve faster transitions but risk added ringing or overshoot. Such trade-offs must be weighed against the latency introduced by purely offline noncausal inverses.

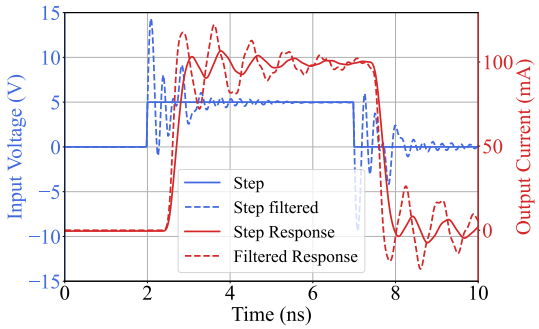

Fig. 11: Input and output waveforms for a magnitude-based, near-minimum-phase inverse filter. Overshoot is more prominent but rise time is improved.

B. PID Control

Finally, a PID-based control approach was investigated to regulate the SOA drive signal in real time. In this scheme, the error signal is reduced through proportional (P) and integral (I) actions, with an anticipatory component added by the derivative (D). The total control input at time index k is given by [8]:

$$\begin{aligned} u[k] &= u_P + u_I + u_D \\ &= K_p\, e[k] + K_i\, e_{\text{int}}[k+1] + K_d\, \frac{e[k] - e[k-1]}{dt} \end{aligned} \tag{2}$$

where K_p, K_i, and K_d are the proportional, integral, and derivative gains, respectively. The term $e[k]$ is the error at the k-th time instant, while $e_{\text{int}}[k+1]$ is the accumulated integral of the error up to $(k+1)$. Figure 12 shows a schematic representation of this control loop.

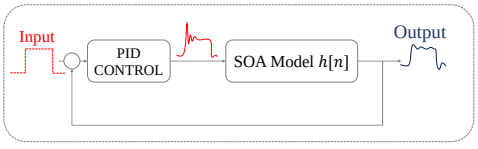

Fig. 12: Schematic diagram of the PID controller applied to the SOA model.

The PID loop is driven by an impulse-response representation of the SOA circuit. At each time step, the controller computes the output current by convolving the past input drive with the impulse response $h[n]$. The difference between the desired (reference) current and the actual current serves as the error to be minimized by the PID. By appropriately tuning K_p, K_i, and K_d, the controller is able to accelerate the SOA's transient response (reducing its rise time) and simultaneously mitigate overshoot.

Figure 13 illustrates an example in which a step-like optical pulse demand is placed at a chosen time instant, and the PID acts to shape the electrical drive signal so that the circuit output more closely follows the target amplitude. As shown, the PID-driven input achieves a smaller overshoot compared to a raw step input, although the degree of improvement depends on the controller gains.

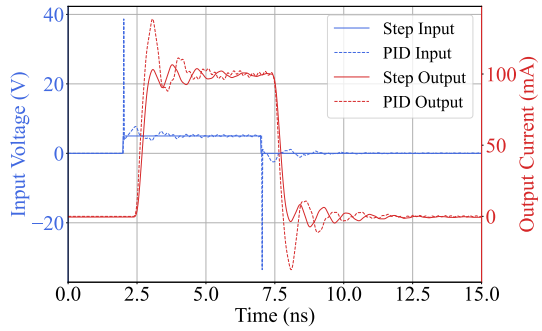

Fig. 13: Comparison of input (PID drive) and output currents using the SOA model with an embedded PID controller.

C. Comparison of the Proposed Techniques

Table II summarizes the main switching parameters for each method, using the plain step input as a baseline. Here, we consider two representative FIR-filtering approaches:

- Filter 1 (Noncausal Inverse): Provides the best rise time and low overshoot, yet introduces significant latency due to its filter length.
- Filter 2 (Causal/Minimum-Phase Inverse): Offers a moderate rise time and slightly higher overshoot compared to Filter 1, but avoids large latency. Its settling time, however, is relatively poorer than the other methods.

Finally, the PID controller shows a balanced performance across all parameters, reducing rise time and overshoot simultaneously, albeit not matching the absolute minimal rise time of Filter 1. Its key advantage is adaptability and minimal imposed latency compared to an offline FIR solution.

TABLE II: Comparison of Switching Parameters for Different Techniques.

Parameter	Step (Baseline)	Filter 1	Filter 2	PID
Rise Time (ps)	320	120	180	260
Overshoot (%)	7.32	4.74	21.29	39.25
Settling Time (ns)	1.82	0.14	4.22	1.76

As shown in Table II, Filter 1 delivers the lowest rise time and keeps overshoot small, but its offline noncausal nature induces a larger latency. Filter 2 provides a good compromise in terms of rise time and simplicity, yet overshoot increases significantly, and the settling time becomes the highest among the investigated approaches. The PID control method offers an intermediate rise time with lower latency than Filter 1, a more modest overshoot than Filter 2, and a settling time that remains competitive compared to the other solutions. Thus, the optimal choice depends on the design priorities among speed, overshoot, settling behavior, and implementation constraints.

IV. Conclusions

This work proposed and validated an algorithm for solving equivalent circuits of semiconductor optical amplifiers. The custom Python-based simulator demonstrated close agreement with commercial results from Ansys Circuit. Additionally, two FIR-based filtering techniques and a PID controller approach were investigated to reduce the SOA switching time and equalize the optical output signal. Comparisons of rise time, overshoot, and settling time were carried out for all three methods. As future work, we intend to evaluate the SOAs' nonlinearities and experimentally validate the proposed techniques.

Aknowledgements

This work received partial funding from Project XGM-AFCCT-2024-7-1-1, supported by xGMobile – EMBRAPII-Inatel Competence Center on 5G and 6G Networks, with financial resources from the PPI IoT/Manufacturing 4.0 program of MCTI (grant number 052/2023), signed with EMBRAPII. The authors also thank the financial support from CNPq (#303595/2021-3, #402081/2023-4, #178452/2024-6, #305777/2022-0), INCT (#408345/2024-1), CAPES, FINEP, FAPEMIG (Contracts #PPE-00124-23, RED-00194-23 and APQ-02746-21) and FAPESP (Contracts #2021/06569-1, #2022/11596-0, #2023/16019-4 and #2022/09319-9).

References

[1] Sutili, Tiago. Aquisição experimental fotoelétrica ultrarrápida com algoritmos de processamento digital para a análise de subsistemas em comunicações ópticas coerentes de altíssimas taxas   . 2018. 1 recurso online (210 p.) Tese (doutorado) - Universidade Estadual de Campinas, Faculdade de Engenharia Elétrica e de Computação, Campinas, SP.

[2] C. M. Gallep and E. Conforti, "Reduction of semiconductor optical amplifier switching times by preimpulse step-injected current technique," in IEEE Photonics Technology Letters, vol. 14, no. 7, pp. 902-904, July 2002, doi: 10.1109/LPT.2002.1012379.

[3] R. C. Figueiredo, N. S. Ribeiro, A. M. O. Ribeiro, C. M. Gallep and E. Conforti, "Hundred-Picoseconds Electro-Optical Switching With Semiconductor Optical Amplifiers Using Multi-Impulse Step Injection Current," in Journal of Lightwave Technology, vol. 33, no. 1, pp. 69-77, 1 Jan.1, 2015, doi: 10.1109/JLT.2014.2372893.

[4] Toazza, Adriano Luís. Chaveamento Eletro-óptico De Amplificadores ópticos a Semicondutor: Experimentos E Modelagem Computacional. 2010.

[5] C. W. F. Parsonson, Z. Shabka, W. K. Chlupka, B. Goh and G. Zervas, "Optimal Control of SOAs With Artificial Intelligence for Sub-Nanosecond Optical Switching," in Journal of Lightwave Technology, vol. 38, no. 20, pp. 5563-5573, 15 Oct.15, 2020, doi: 10.1109/JLT.2020.3004645.

[6] H. Alkharsan, C. W. F. Parsonson, Z. Shabka, X. Mu, A. Ottino and G. Zervas, "Optimal and Low Complexity Control of SOA-Based Optical Switching with Particle Swarm Optimisation," 2022 European Conference on Optical Communication (ECOC), Basel, Switzerland, 2022, pp. 1-4.

[7] L. R. R. Dos Santos, F. R. Durand, A. Goedtel and T. Abrao, "Auto-tuning PID distributed power control for next-generation passive optical networks," in Journal of Optical Communications and Networking, vol. 10, no. 10, pp. D110-D125, Oct. 2018, doi: 10.1364/JOCN.10.00D110.

[8] OGATA, Katsuhiko. Engenharia de controle moderno. 5. ed. Pearson, 2010.

[9] R. S. Tucker and D. J. Pope, "Microwave Circuit Models of Semiconductor Injection Lasers," in IEEE Transactions on Microwave Theory and Techniques, vol. 31, no. 3, pp. 289-294, Mar. 1983, doi: 10.1109/TMTT.1983.1131478.

[10] S. Haykin, Adaptive Filter Theory, 5th ed. Upper Saddle River, NJ, USA: Prentice Hall, 2013.